Journal of Hazardous Materials 177 (2010) 554–559

Contents lists available at ScienceDirect

Journal of Hazardous Materials

journal homepage: www.elsevier.com/locate/jhazmat

Combustion synthesis and effect of $LaMnO_3$ and $La_{0.8}Sr_{0.2}MnO_3$ on RDX thermal decomposition

Zhi-Xian Wei [a,*], Lin Wei [a], Lin Gong [a], Yan Wang [a], Chang-Wen Hu [b,*]

[a] Department of Chemistry, Science Institute, North University of China, Taiyuan, Shanxi 030051, PR China
[b] Department of Chemistry and the Institute for Chemical Physics, Beijing Institute of Technology, Beijing 100081, PR China

ARTICLE INFO

Article history:
Received 4 September 2009
Received in revised form 4 December 2009
Accepted 13 December 2009
Available online 22 December 2009

Keywords:
Stearic acid gel combustion synthesis
Perovskite-type $La_{0.8}Sr_{0.2}MnO_3$
RDX

ABSTRACT

Perovskite-type $LaMnO_3$ and $La_{0.8}Sr_{0.2}MnO_3$ with high specific surface areas were prepared by stearic acid gel combustion method. The obtained powders were characterized by XRD, FT-IR, SEM and XPS techniques. Their catalytic activities were investigated on thermal decomposition of hexahydro-1,3,5-trinitro-1,3,5-triazine (RDX) by TG-DSC techniques. The experimental results show that $LaMnO_3$ is a more effective catalyst than $La_{0.8}Sr_{0.2}MnO_3$ for the sublimation and melting process of RDX because of its higher concentration ratio of surface-adsorbed species. And the catalytic activity of $La_{0.8}Sr_{0.2}MnO_3$ is higher than that of $LaMnO_3$ for thermal decomposition of liquid RDX. This could be attributed to its higher concentration ratios of surface oxygen and Mn^{4+}/Mn^{3+}. In conclusion, the concentration ratios of surface oxygen and Mn^{4+}/Mn^{3+} could play key roles for RDX thermal decomposition. This study points out a potential way to develop new and more active perovskite-type catalysts for the RDX thermal decomposition.

1. Introduction

ABO_3 perovskite-type oxides with A as La, B as transition metal are widely used in many fields. In particular, they can display prominent catalytic activities. For example, they have been used as catalysts for the auto-reforming of sulfur containing fuels [1] for removal of ethylacetate, CO and NO_x [2] and for the total oxidation of methane and Volatile Organic Compounds [3]. However, one of the technical constraints to the use of perovskite-type catalysts is the inability to produce high specific surface area powders [4].

Structures and properties of ABO_3 oxides are strongly influenced by the synthetic methods. The $LaMnO_3$ and related compounds have been synthesized by many methods, including sol–gel method, flame hydrolysis from aqueous solution, complexation through EDTA as well as solid-state reaction [5] and solution combustion synthesis [6]. In this study, we prepared perovskite-type $LaMnO_3$ and $La_{0.8}Sr_{0.2}MnO_3$ with high specific surface areas by stearic acid gel combustion method, where stearic acid was used as reaction solvent, dispersant, complexing agent.

Hexahydro-1,3,5-trinitro-1,3,5-triazine (RDX) is the key energetic material and the most common oxidizer in the rocket propellant. Considering the limited loading of RDX and its composites in the rocket, it is crucial for us to further improve its decomposition efficiency to produce large amount of energy as far as possible and to decrease its burning temperature for easy operation and control. So, catalysis of RDX thermal decomposition is of interest. Some additives or catalysts such as nanodiamond/Cu [7,8], nano-$LaCoO_3$ [9], and nanometer-sized lanthanum oxide [10] have been proved effective to improve the decomposition or explosion of RDX. In order to search more additives or catalysts for RDX thermal decomposition, $LaMnO_3$ and $La_{0.8}Sr_{0.2}MnO_3$ were prepared and investigated for RDX thermal decomposition in this study. These researches are not only favorable for the controlled preparation of $LaMnO_3$ and $La_{0.8}Sr_{0.2}MnO_3$, but also for the deep understanding of their effect on the decomposition of RDX.

2. Experimental

2.1. Auto-combustion synthesis of perovskite-type $LaMnO_3$

$MnCl_2{\cdot}4H_2O$, $La(NO_3)_3{\cdot}6H_2O$ and stearic acid were used as raw materials to prepare $LaMnO_3$ powder. First, $MnCl_2{\cdot}4H_2O$ and $La(NO_3)_3{\cdot}6H_2O$ with Mn/La molar ratio of 1/1 were added into the excess of 8.0–10.0% molten stearic acid in a porcelain crucible reactor. After that, the resulting mixture was continuously stirred and kept at 118 °C for a sufficient period of time to allow the La-Mn-stearic acid gel to be formed. Then, the porcelain crucible reactor was placed on a hot plate increased to 500 °C. At this stage, the gel volatilized and autoignited, with the evolution of a large volume of gases to produce loose powder, after the loose powder was calcined at 700 °C for 1 h, perovskite-type $LaMnO_3$ was obtained.

* Corresponding authors. Tel.: +86 0351 3921414; fax: +86 0351 3921414.
E-mail address: zx_wei@126.com (Z.-X. Wei).

0304-3894/$ – see front matter © 2009 Elsevier B.V. All rights reserved.
doi:10.1016/j.jhazmat.2009.12.068

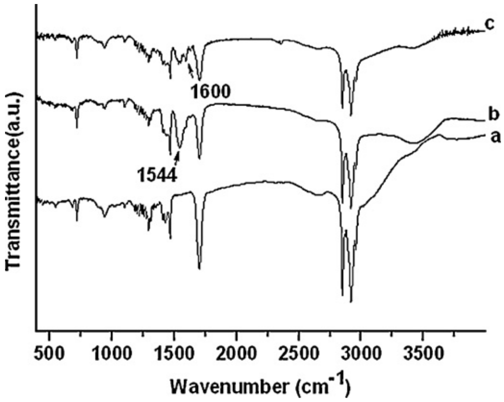

Fig. 1. FT-IR spectra of stearic acid (a), La-Sr-Mn-stearic acid gel (b), La-Mn-stearic acid gel (c).

2.2. *Auto-combustion synthesis of perovskite-type $La_{0.8}Sr_{0.2}MnO_3$*

Perovskite-type $La_{0.8}Sr_{0.2}MnO_3$ powder was synthesized using $La(NO_3)_3{\cdot}6H_2O$, $SrCO_3$, $MnCl_2{\cdot}4H_2O$ and stearic acid as raw materials according to the same procedures and experimental conditions as were described for the preparation of $LaMnO_3$. Here, the molar ratio of $La(NO_3)_3{\cdot}6H_2O$:$SrCO_3$:$MnCl_2{\cdot}4H_2O$ is 0.8:0.2:1, the molten stearic acid is the excess of 8.0–10.0%. After the loose powder obtained by combustion of La-Sr-Mn-stearic acid gel was calcined at 600 °C for 2 h, the perovskite-type $La_{0.8}Sr_{0.2}MnO_3$ was formed.

2.3. *Powders characterization*

The composition and phase purity of obtained powders were examined by X-ray diffractometer (CuK_α = 1.54 Å, 40 kV, 30 mA, 2θ from 10° to 80°). FT-IR spectra were registered by using a Nexus 870 FT-IR in KBr pellets. The BET specific surface areas of the obtained powders were evaluated from the linear parts of the BET plot of the N_2 isotherms, using a NOVA4200e analyzer. Scanning electron microscopy (SEM) (HITACHA, Model S-4800) was used to investigate the morphology of obtained powders. XPS analysis was performed by a PHI Quantera SXM apparatus, equipped with a standard Al Ka excitation source. The binding energy (BE) scale has been calibrated by measuring C1*s* peak (BE = 284.8 eV) from the ubiquitous surface layer of adventitious carbon.

2.4. *Catalytic activity test*

The obtained powders and RDX were mixed in 2:98 (wt.%) respectively by rubbing method to prepare the samples for TG-DSC experiments. The samples were placed in a 40 μL Al pan and covered with a piercing Al lid. The experiments were carried out at heating rates of 10 °C min^{-1} on a NETZSCH STA 449C and about 2 mg of sample was used. N_2 was used as the carrier gas at a flow rate of 50 mL min^{-1}.

3. Results and discussion

3.1. *FT-IR analysis*

FT-IR spectra of stearic acid, La-Sr-Mn-stearic acid gel and La-Mn-stearic acid gel are shown in Fig. 1. Comparing Fig. 1b and c with a, one can see that a new band 1544 cm^{-1} for La-Sr-Mn-stearic acid gel and two new band 1544 cm^{-1} and 1600 cm^{-1} for La-Mn-stearic acid gel were observed, which is assigned to the stretching vibration of –COO. These results indicate that stearic acid replaced NO_3^-, Cl^- and CO_3^{2-} to complex with metal ions after the corresponding salts were added into the melted stearic acid, and a strong coordination interaction between salts and stearic acid exist, indicating stearic acid was used as complexing agent.

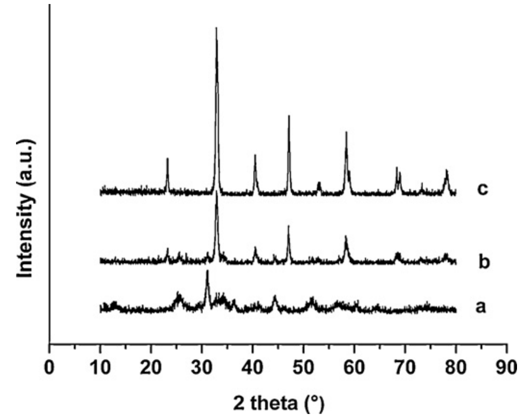

Fig. 2. XRD of obtained powders: LaOCl powder mixture (a), LaOCl powder mixture calcained at 600 °C (b), perovskite-type $LaMnO_3$ calcained at 700 °C (c).

3.2. *Phase composition and microstructure of $LaMnO_3$ and $La_{0.8}Sr_{0.2}MnO_3$*

The X-ray diffraction patterns of the powders obtained by combustion of La-Mn-stearic acid gel are shown in Fig. 2. The broad and poorly defined peaks in Fig. 2a correspond to LaOCl (PDF # 64-7261). So, the loose powder obtained by the combustion of the La-Mn-stearic acid gel is a mixture of LaOCl and significant amounts of amorphous materials. The LaOCl peaks are also present after heating to 600 °C (Fig. 2b) and, additionally, intense peaks associated with the cubic perovskite structure emerge. By 700 °C, the LaOCl has completely decomposed and the single-phase perovskite-type $LaMnO_3$ (PDF # 75-0440, cubic, a = 3.880) is formed.

Fig. 3 shows the X-ray diffraction patterns of the powders obtained by combustion of La-Sr-Mn-stearic acid gel. The broad and poorly defined peaks in Fig. 3a correspond to LaOCl (PDF # 64-7261). So, the loose powder obtained by the combustion of the La-Sr-Mn-stearic acid gel is also a mixture of LaOCl and significant amounts of amorphous materials. The LaOCl peaks are still present after heating to 600 °C for 1 h (Fig. 3b), but intense peaks associated with the perovskite-type $La_{0.8}Sr_{0.2}MnO_3$ structure emerge. By 600 °C for 2 h, the LaOCl has completely decomposed and perovskite-type $La_{0.8}Sr_{0.2}MnO_3$ peaks are formed. The perovskite-

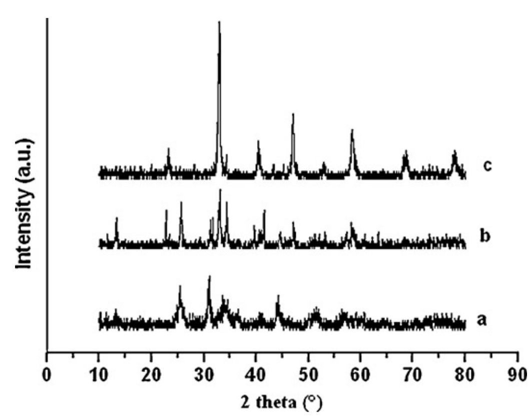

Fig. 3. XRD of obtained powders: LaOCl powder mixture (a), LaOCl powder mixture calcained at 600 °C for 1 h (b), perovskite-type $La_{0.8}Sr_{0.2}MnO_3$ calcained at 600 °C for 2 h (c).

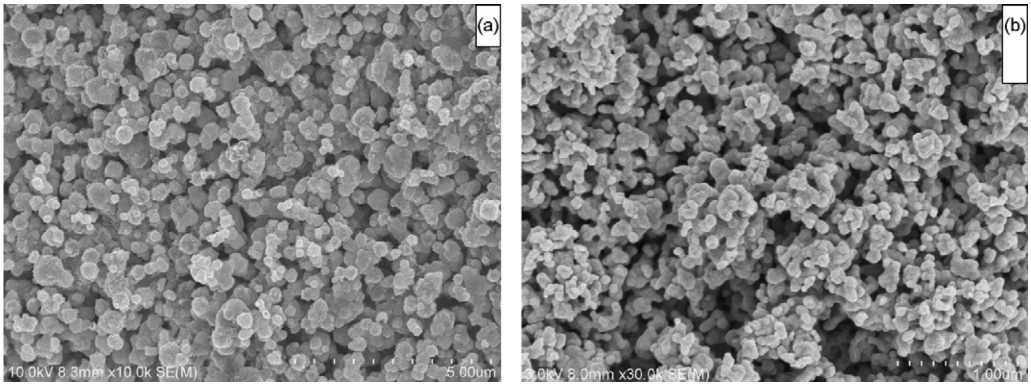

Fig. 4. SEM of obtained powders: $La_{0.8}Sr_{0.2}MnO_3$ ×10K (a) and $LaMnO_3$ ×30K (b).

type $La_{0.8}Sr_{0.2}MnO_3$ exhibits rhombohedral symmetry, space group R3c (PDF # 167).

Fig. 4 shows the SEM images of $LaMnO_3$ and $La_{0.8}Sr_{0.2}MnO_3$. It can be seen that $La_{0.8}Sr_{0.2}MnO_3$ and $LaMnO_3$ are almost-spherical nano-agglomerates with characteristic scale ~0.25–0.5 μm (Fig. 4a) and ~0.05–0.1 μm (Fig. 4b), respectively. Moreover, the SEM images reveal a uniform grain size distributions and homogeneous microstructures.

In this study, the specific surface areas of $LaMnO_3$ calcained at 700 °C for 1 h and $L_{0.8}Sr_{0.2}MnO_3$ calcained at 600 °C for 2 h are 26.76 m^2/g and 12.62 m^2/g, respectively. However, the corresponding values for $LaMnO_3$ prepared by oxalyl dihydrazide and urea aqueous solution combustion methods are 12.5 m^2/g [11], 5.6 m^2/g [12], respectively; the values for $La_{0.8}Sr_{0.2}MnO_3$ obtained by citric acid combustion synthesis and the amorphous citrate process are 11.53 m^2/g [13], 5.1 m^2/g [14], respectively. Obviously, the values in this study are higher. This is because that the formation of gel is in the non-aqueous medium of stearic acid. This is helpful to prevent the hydrolysis of the metal ions and make a well-premixed gel, resulting in the better crystallized structures and high specific surface areas. In addition, the long-chain structure of stearic acid has been used as the dispersion and lead to the formation of the powders with high specific surface areas. Therefore, stearic acid gel combustion is an effective way to prepare nanometer/ultrafine powders.

3.3. FT-IR spectra

In the FT-IR spectra of $LaMnO_3$ and $La_{0.8}Sr_{0.2}MnO_3$ (Figure 1s, Supporting Information), the wide bands observed at about 3466 cm^{-1} are characteristic of the H–O bending mode of absorbed water or hydroxyl groups, and the bands observed at about 2359 cm^{-1} correspond to the physically surface-absorbed CO_2 (due to the deformation mode of gas-phase CO_2, unperfectly subtracted). The band at 1637 cm^{-1} corresponds to the surface-adsorbed oxygen species (O_{ad}) [15], and the bands at 614 cm^{-1} correspond to the stretching mode of the Mn–O–Mn or Mn–O bond [11]. These results showed that the adsorbed water or hydroxyl groups, surface-adsorbed oxygen exist on the surface of $LaMnO_3$ and $La_{0.8}Sr_{0.2}MnO_3$.

3.4. XPS studies

Fig. 5 shows the C1*s* spectra of $La_{0.8}Sr_{0.2}MnO_3$ (a) and $LaMnO_3$ (b). C1*s* signal in Fig. 5a and b located at 284.9 eV corresponds to the reference, and the higher one (around 288.8 eV) can be assigned to carbonated species. Since La and Sr-based perovskites are basic materials, they are easily carbonated in air [14]. However, carbonate phases have not been detected by XRD in this study. This conflict can be resolved by considering the different sampling depth of the two analytical techniques: XRD is in fact a bulk technique, while XPS is a surface technique characterized by a sampling.

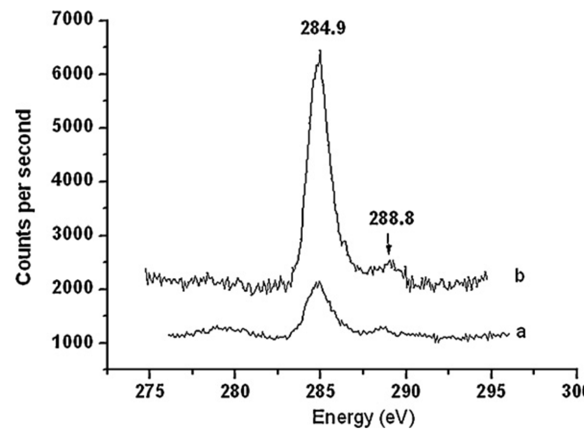

Fig. 5. C1*s* XP spectra of $La_{0.8}Sr_{0.2}MnO_3$ (a) and $LaMnO_3$ (b).

Fig. 6 shows the O1*s* spectra of $La_{0.8}Sr_{0.2}MnO_3$ (a) and $LaMnO_3$ (b). In Fig. 6b, O1*s* spectra of $LaMnO_3$ show two major components: one at 529.4 eV is attributable to the lattice oxygen O^{2-}, and the other broad peak at around 531.6 eV corresponds to surface-adsorbed oxygen species. Based on the results of FT-IR (Figure 1s, Supporting Information) and the C1*s* XP spectra of $La_{0.8}Sr_{0.2}MnO_3$ and $LaMnO_3$ (Fig. 5), the surface-adsorbed oxygen species consist of adsorbed oxygen (O_{ad}), hydroxyl groups or water and carbonate species. For $La_{0.8}Sr_{0.2}MnO_3$, O1*s* spectra (Fig. 6a)

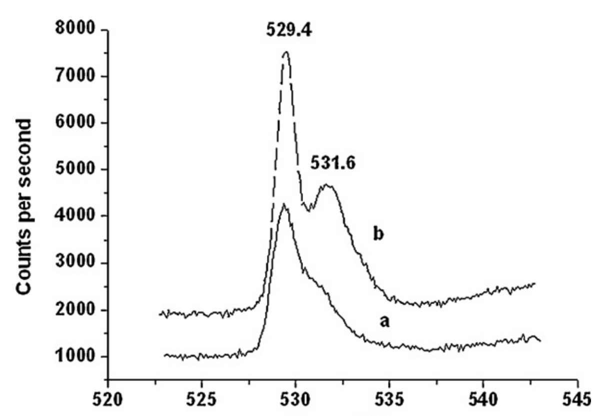

Fig. 6. O1*s* XP spectra of $La_{0.8}Sr_{0.2}MnO_3$ (a) and $LaMnO_3$ (b).

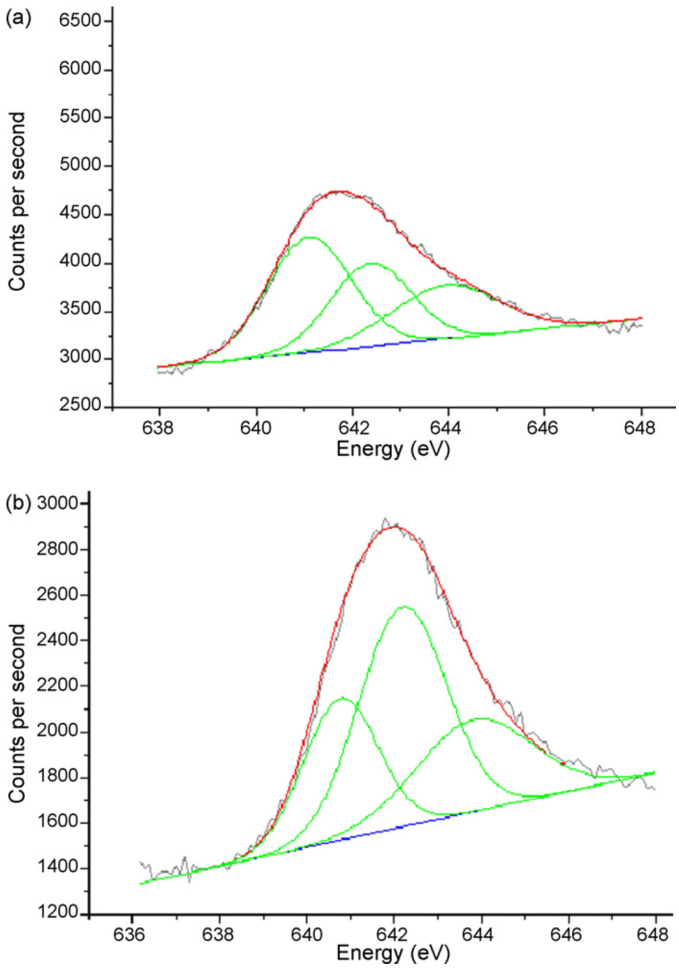

Fig. 7. Mn 2*p*3/2 XP spectra of $LaMnO_3$ (a) and $La_{0.8}Sr_{0.2}MnO_3$ (b).

indicates two major components: one at 529.4 eV is attributable to the lattice oxygen O^{2-}, and the other peak at around 531.6 eV corresponds to the surface-adsorbed species, which are also comprised of adsorbed oxygen (O_{ad}), hydroxyl groups or water and carbonate species. A comparison of Fig. 6a and b replies that $LaMnO_3$ has much higher surface-adsorbed species.

It is well known that the partial substitution of La^{3+} by a divalent element in $LaMnO_3$ may introduce a mixture system of Mn^{3+} and Mn^{4+} ions. Fig. 7 shows the Mn 2*p*3/2 spectra of Mn 2*p* XP spectra of $LaMnO_3$ (a) and $La_{0.8}Sr_{0.2}MnO_3$ (b). The Mn 2*p*3/2 is broad and asymmetric towards the high binding energy side. Peak intensities were evaluated by applying a peak synthesis procedure that includes three components, namely Mn^{4+} (642.4 eV), Mn^{3+} (641.3 eV) and a satellite (644 eV). It should be emphasised at this point that the deconvolution method yields ambiguity in the recognition of the Mn^{4+} and Mn^{3+} species due to the small differences in their binding energy values [16].

The different atomic concentration ratios on the surface of $La_{0.8}Sr_{0.2}MnO_3$ and $LaMnO_3$ were calculated and listed in Table 1.

Table 1
Surface atomic concentration ratios for $LaMnO_3$ and $La_{0.8}Sr_{0.2}MnO_3$.

$La_{0.8}Sr_{0.2}MnO_3$	Surface oxygen/M_1 48.68	Mn^{4+}/Mn^{3+} 1.77	Mn/M_1 12.65
$LaMnO_3$	Surface oxygen/M_2 36.44	Mn^{4+}/Mn^{3+} 0.69	Mn/M_2 6.28

M_1: total amount of La + Mn + Sr cations + O anion + C for $La_{0.8}Sr_{0.2}MnO_3$; M_2: total amount of La + Mn cations + O anion + C for $LaMnO_3$.

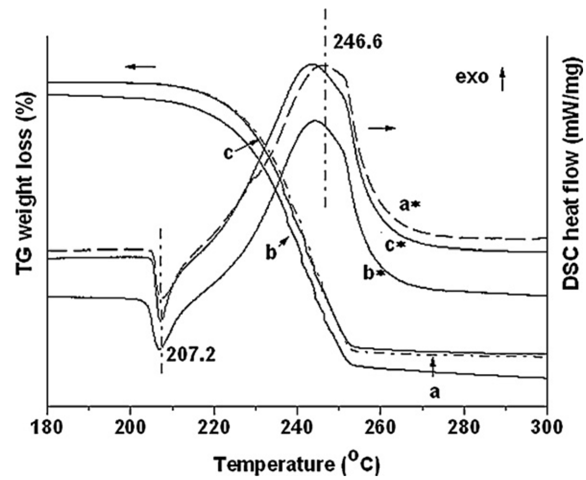

Fig. 8. TG-DSC curves of catalytic thermal decomposition of RDX at a 10 °C min^{-1} in nitrogen: RDX. [a (TG), a* (DSC)], RDX + $LaMnO_3$ [b (TG), b* (DSC)], RDX + $La_{0.8}Sr_{0.2}MnO_3$ [c (TG), c* (DSC)].

Table 1 indicates that the concentration ratio of surface oxygen (lattice oxygen + adsorbed oxygen species) of $LaMnO_3$ is much lower than those of $La_{0.8}Sr_{0.2}MnO_3$, although its concentration ratio of surface-adsorbed oxygen species is far higher (Fig. 6). And the Mn^{4+}/Mn^{3+} and Mn/M1 ratios of $La_{0.8}Sr_{0.2}MnO_3$ are higher than those of $LaMnO_3$. This indicates that the surface layer of $La_{0.8}Sr_{0.2}MnO_3$ displayed higher oxygen and Mn^{4+}/Mn^{3+} concentration ratios than those of $LaMnO_3$. This is critically important to its catalytic activity.

3.5. Catalytic thermal decomposition of RDX

The catalytic activities of $La_{0.8}Sr_{0.2}MnO_3$ and $LaMnO_3$ for the thermal decomposition of RDX were studied by TG-DSC (Fig. 8). In all the figures, the shift of DSC and TG baseline based on many detections carried out on the same instrument were observed. As shown in Fig. 8a*, a sharp endothermal peak in DSC curve that appears between 180 and 212 °C, corresponding to a weight loss of 1.5%, was assigned to the sublimation and the melting process of RDX [17], After mixing the $LaMnO_3$ and $La_{0.8}Sr_{0.2}MnO_3$ with RDX, the onset temperature in the TG curve shifted from 205.5 °C (RDX) to 204.1 °C and 205.3 °C, respectively, while the weight loss of the RDX with $LaMnO_3$ increased from 1.5% (RDX) to 2.5%, but that of RDX with $La_{0.8}Sr_{0.2}MnO_3$ does not increase in the corresponding temperature range. Here, the weight loss of RDX with $LaMnO_3$ is 1% more than that of RDX with $La_{0.8}Sr_{0.2}MnO_3$. This is likely attributed to the higher concentration ratio of surface-adsorbed species at $LaMnO_3$ surface (Fig. 6). In addition, the melting temperature of RDX with $LaMnO_3$ is at 206 °C, which decreases by 1.2 °C, while the temperature with $La_{0.8}Sr_{0.2}MnO_3$ does not change obviously. This indicates that $LaMnO_3$ is a more effective catalyst than $La_{0.8}Sr_{0.2}MnO_3$ for the sublimation and melting process of RDX.

In the DSC curve of RDX, a broad exothermal peak at 246.6 °C is assigned to the decomposition of liquid RDX in nitrogen. The changes in the exothermic peak have been observed. The exothermic peak in presence of $LaMnO_3$ and $La_{0.8}Sr_{0.2}MnO_3$ shifted from 246.6 °C (RDX) to 244.5 °C and 243.3 °C, respectively. Moreover, it can also be seen from DSC curves that the peaks between 246.6 °C and 252 °C become precipitous in presence of $LaMnO_3$ and $La_{0.8}Sr_{0.2}MnO_3$, indicating that $LaMnO_3$ and $La_{0.8}Sr_{0.2}MnO_3$ could accelerate the reactions between CO and NO or oxidation of CO. Note that CO and NO_x are two major products of RDX thermal decomposition. Further, the decomposition heats of RDX are simultaneously quantitatively determined from the DSC curves with and without $LaMnO_3$ and $La_{0.8}Sr_{0.2}MnO_3$ powders. Adding 2 wt.% $LaMnO_3$ and $La_{0.8}Sr_{0.2}MnO_3$ allows the change of the apparent decomposition heat from 559.7 J/g to 565 J/g and 624.6 J/g, respectively. These data indicate that both $LaMnO_3$ and $La_{0.8}Sr_{0.2}MnO_3$ have catalytic activities, and $La_{0.8}Sr_{0.2}MnO_3$ is a more effective catalyst than $LaMnO_3$ on the thermal decomposition of liquid RDX.

Comparing thermal decomposition mechanism of RDX has a deep understanding of the effect of the catalysts on the thermal decomposition of RDX. Ab Initio Density Functional of RDX [18] indicates that the initiation of RDX decomposition by N-NO_2 homolysis and propagation of the decomposition by hydrogen atom abstractions should be facile processes. It is reported that hydrogen atoms in HMX may be abstracted by radicals present in the gas-phase, such as OH and water [19]. Water is one of the most abundant species during octahydro-1,3,5,7-tetranitro-1,3,5,7-tetrazocine (HMX) and RDX thermal decomposition. So, Behrens concluded that OH and H_2O may initiate HMX thermal decomposition [19]. In consideration of the similar structure and decomposition mechanism of RDX and HMX [18,19], one could conclude that OH and H_2O could also initiate RDX thermal decomposition. Moreover, surface-adsorbed species such as adsorbed oxygen (O_{ad}), hydroxyl groups or water, are weakly bounded on the powder surface and usually are considerate as the origin of the characteristic catalytic properties [20]. So, one can explain the possible reason of the catalytic effect of $LaMnO_3$ and $La_{0.8}Sr_{0.2}MnO_3$ for the sublimation and melting process of RDX. During the thermal decomposition of RDX in presence of $LaMnO_3$ and $La_{0.8}Sr_{0.2}MnO_3$ with increasing temperature, the desorbed gases such as H_2O and O_2, which may come from surface-adsorbed H_2O, OH^- and adsorbed oxygen (O_{ad}), could abstract the hydrogen atoms from RDX, resulting in accelerating the sublimation and melting process of RDX. $LaMnO_3$ with a higher concentration ratio of surface-adsorbed species (Fig. 6) yields a higher catalytic activity.

The specific surface area of $La_{0.8}Sr_{0.2}MnO_3$ (12.62 m^2/g) is lower than that of $LaMnO_3$ (26.76 m^2/g). This does not help to explain the better catalytic activity of $La_{0.8}Sr_{0.2}MnO_3$ for thermal decomposition of liquid RDX. To understand this, it is also necessary to analyze the surface atomic concentration ratios of $LaMnO_3$ and $La_{0.8}Sr_{0.2}MnO_3$ and decomposition mechanism of RDX. During the thermal decomposition of RDX in presence of $LaMnO_3$ and $La_{0.8}Sr_{0.2}MnO_3$ with increasing temperature, some surface-adsorbed species were desorbed and exposed lattice species such as Mn ion and lattice oxygen. The lattice oxygen, the remanent surface-adsorbed oxygen (O_{ad}) and Mn ions with different oxidation states are critically important to the oxidation reaction of CO and the reaction between CO and NO [21–23]. These oxidation reaction can be catalyzed by $LaMnO_3$ [21] and $La_{0.8}Sr_{0.2}MnO_3$ [22]. These rapid exothermic reactions may accelerate the decomposition of RDX and result in the increase of the decomposition heat. $La_{0.8}Sr_{0.2}MnO_3$ with higher concentration ratios of surface oxygen and Mn^{4+}/Mn^{3+} (Table 1) yields a higher catalytic activity.

4. Conclusion

Perovskite-type $LaMnO_3$ and $La_{0.8}Sr_{0.2}MnO_3$ with high specific surface areas were prepared by stearic acid gel combustion route. RDX catalytic thermal decomposition reveals that both perovskite-type $LaMnO_3$ and $La_{0.8}Sr_{0.2}MnO_3$ have catalytic activities; $LaMnO_3$ has higher catalytic activity than $La_{0.8}Sr_{0.2}MnO_3$ for the sublimation and melting process of RDX because of its higher surface-adsorbed oxygen (O_{ad}) and hydroxyl. And $La_{0.8}Sr_{0.2}MnO_3$ has higher catalytic activity than $LaMnO_3$ for thermal decomposition of liquid RDX. This could be attributed to its higher concentration ratios of surface oxygen and Mn^{4+}/Mn^{3+}. In conclusion, the concentration ratios of surface oxygen and Mn^{4+}/Mn^{3+} could play key roles for RDX thermal decomposition.

For perovskite-type oxides ABO_3, oxygen vacancies and metal ions with different oxidation states can be generated by A-site replacements and through the modification of B-site ion oxidation states by ion substitutions in A- and/or B-sites. As a result of the combined effect, one can design and prepare perovskite-type oxides with more active oxygen and B ions with different oxidation states. Thus, studies based on combinatorial perovskite-type oxide catalysis for RDX thermal decomposition are in progress in our laboratory.

Acknowledgement

This project was supported by the Natural Science Fund Council of China (NSFC, Nos. 20671084, 20671011 and 20731002).

Appendix A. Supplementary data

Supplementary data associated with this article can be found, in the online version, at doi:10.1016/j.jhazmat.2009.12.068.

References

[1] P. Dinka, Alexander, S. Mukasyan, Perovskite catalysts for the auto-reforming of sulfur containing fuels, J. Power Sources 167 (2007) 472–481.

[2] J.R. Niu, J.G. Deng, W. Liu, L. Zhang, G.Z. Wang, H.X. Dai, H. He, X.H. Zi, Nanosized perovskite-type oxides $La_{1-x}Sr_xMo_{3-\delta}$ (M = Co, Mn; x = 0, 0.4) for the catalytic removal of ethylacetate, Catal. Today 126 (2007) 420–429.

[3] A. Delmastro, D. Mazza, S. Ronchetti, M. Vallino, R. Spinicci, P. Brovetto, M. Salis, Synthesis and characterization of non-stoichiometric $LaFeO_3$ perovskite, Mater. Sci. Eng. B: Solid State Mater. Adv. Technol. 79 (2001) 140–145.

[4] J. Shu, S. Kaliaguine, Well-dispersed perovskite-type oxidation catalysts, Appl. Catal. B: Environ. 16 (1998) L303–L308.

[5] E. Campagnoli, A. Tavaresb, L. Fabbrini, I. Rossetti, Yu.A. Dubitsky, A. Zaopo, L. Forni, Effect of preparation method on activity and stability of $LaMnO_3$ and $LaCoO_3$ catalysts for the flameless combustion of methane, Appl. Catal. B: Environ. 55 (2005) 133–139.

[6] A. Civera, G. Negro, S. Specchia, G. Saracco, V. Specchia, Optimal compositional and structural design of a $LaMnO_3/ZrO_2$/Pd-based catalyst for methane combustion, Catal. Today 100 (2005) 275–281.

[7] X.P. Fan, X. Wang, Z.R. Liu, H.M. Tan, Catalysis of nano Cu powder on the thermal decomposition of HMX and RDX, Energy Mater. (Chin.) 13 (2005) 284–287.

[8] X.Q. Shi, I.H. Jiang, L.D. Lu, X.J. Yang, X. Wang, Structure and catalytic activity of nanodiamond/Cu nanocomposites, Mater. Lett. 62 (2008) 1238–1241.

[9] A.L. Xue, Y.S. Huang, C.C. Kang, Y.H. Wang, J. Li, The Effect of nano-$LaCoO_3$ on the thermal decomposition and sensitivity of RDX explosive mixture, J. Explos. Propell. (Chin.) 28 (2005) 75–77.

[10] H. Xu, J.H. Liu, P. Chen, F.Q. Zhao, D.Y. Tian, Effect of nanometer-sized lanthanum oxide on catalyzing decomposition of cyclotrimethylenetriamine, J. Propul. Technol. (Chin.) 23 (2002) 329–331.

[11] B.M. Nagabhushana, R.P. Sreekanth Chakradhar, K.P. Ramesh, C. Shivakumara, G.T. Chandrappa, Combustion synthesis, characterization and metal–insulator transition studies of nanocrystalline $La_{1-x}Ca_xMnO_3$ ($0.0 \le x \le 0.5$), Mater. Chem. Phys. 102 (2007) 47–52.

[12] A. Civera, M. Pavese, G. Saracco, V. Specchia, Combustion synthesis of perovskite-type catalysts fornatural gas combustion, Catal. Today 83 (2003) 199–211.

[13] C.J. Fu, K.N. Su, N.Q. Zhang, D.R. Zhou, Preparation of ultrafine $La_{0.8}Sr_{0.2}MnO_{3-\delta}$ powders by low temperature combustion synthesis, J. Funct. Mater. (Chin.) 37 (2006) 25–928.

[14] S. Ponce, M.A. Peña, J.L.G. Fierro, Surface properties and catalytic performance in methane combustion of Sr-substituted lanthanum manganites, Appl. Catal. B: Environ. 24 (2004) 193–205.

[15] L. Wu, J.C. Yu, L.Z. Zhang, X.C. Wang, S.K. Li, Selective self-propagating combustion synthesis of hexagonal and orthorhombic nanocrystalline yttrium iron oxide, J. Solid State Chem. 177 (2004) 3666–3674.

[16] K. Barbara, T. Włodzimierz, Partial substitution of lanthanum with silver in the $LaMnO_3$ perovskite: effect of the modification on the activity of monolithic catalysts in the reactions of methane and carbon oxide oxidation, Appl. Catal. A: Gen. 335 (2008) 28–36.

[17] G.T. Long, S. Vyazovkin, B.A. Brems, C.A. Wight, Competitive vaporization and decomposition of liquid RDX, J. Phys. Chem. B 104 (2000) 2570–2574.

[18] J.H. Nathan, L. Koop, Ab initio density functional computations of conformations and bond dissociation energies for hexahydro-1,3,5-trinitro-1,3,5-triazine, J. Am. Chem. Soc. 119 (1997) 6583–6589.

[19] R. Behrens Jr., Thermal decomposition of energetic materials: temporal behaviors of the rates of formation of the gaseous pyrolysis products

from condensed-phase decomposition of octahydro-l,3,5,7-tetranitro-l,3,5,7-tetrazocine, J. Phys. Chem. 94 (1990) 6706–6718.
[20] M.A. Peña, J.L.G. Fierro, Chemical structures and performance of perovskite oxides, Chem. Rev. 101 (2001) 1981–2018.
[21] A.E. Giannakas, A.K. Ladavos, P.J. Pomonis, Preparation, characterization and investigation of catalytic activity for NO + CO reaction of $LaMnO_3$ and $LaFeO_3$ perovskites prepared via microemulsion method, Appl. Catal. B: Environ. 49 (2004) 147–158.
[22] P.Y. Lin, Y.L. Fu, S.M. Yu, An approach to the oxidation reaction mechanism of CO on $La_{0.5}Sr_{0.5}MnO_3$, J. Catal. (Chin.) 2 (1981) 186–193.
[23] F. Teng, W. Han, S.H. Liang, B. Gaugeu, R.L. Zong, Y.F. Zhu, Catalytic behavior of hydrothermally synthesized $La_{0.5}Sr_{0.5}MnO_3$ single-crystal cubes in the oxidation of CO and CH_4, J. Catal. 250 (2007) 1–11.